Biomedicine & Pharmacotherapy 82 (2016) 327–336

Available online at
ScienceDirect
www.sciencedirect.com

Elsevier Masson France
EM|consulte
www.em-consulte.com/en

Synthesis and photodynamic activity of unsymmetrical A_3B tetraarylporphyrins functionalized with L-glutamate and their Zn(II) and Cu(II) metal complex derivatives

Eder U. Arredondo-Espinoza, Susana T. López-Cortina, Mónica A. Ramírez-Cabrera, Isaías Balderas-Rentería*

Universidad Autónoma de Nuevo León, Laboratorio de Ingeniería Genética y Genómica, Facultad de Ciencias Químicas, Av. Universidad s/n, Cd. Universitaria, 66451 San Nicolás de los Garza, N.L., Mexico

ARTICLE INFO

Article history:
Received 27 December 2015
Received in revised form 7 May 2016
Accepted 9 May 2016

Keywords:
L-glutamate
Metalloporphyrins
Photodynamic therapy
Photosensitizer
Unsymmetrical porphyrins

ABSTRACT

Four novel unsymmetrical A_3B porphyrins **1**, **2**, **3** and **4** were synthesized following Lindsey procedure. Porphyrins **3** and **4** include one and three l-glutamate groups, respectively, and all porphyrins were metallated with Zn(II) (**1a–4a**) or Cu(II) (**1b–4b**). Porphyrins and metalloporphyrins presented values of singlet oxygen quantum yields (ΦD) ranging from 0.21 to 0.67. The tetraaryl derivatives in this study showed phototoxicity in SiHa cells with IC_{50} values ranging from <0.01 to $6.56 \pm 0.11\ \mu M$, the metalloporphyrin **4a** showed the lowest IC_{50} value. Comparing the phototoxic activity between all porphyrins, functionalization of porphyrins with glutamate increased 100 times phototoxic activity (**1** (IC_{50} $4.81 \pm 0.34\ \mu M$) vs. **3** (IC_{50} $0.04 \pm 0.02\ \mu M$) and **2** (IC_{50} $5.19 \pm 0.42\ \mu M$) vs. **4** (IC_{50} $0.05 \pm 0.01\ \mu M$)). This increased activity could be attributed to reduced hydrophobicity and increased $\Phi\Delta$, given by functionalization with l-glutamate. Metalloporphyrins **3a** (IC_{50} $0.04 \pm 0.01\ \mu M$) and **4a** ($IC_{50} < 0.01\ \mu M$) presented the best values of phototoxic activity. Therefore, functionalization and zinc metalation increased the phototoxic activity. SiHa cells treated with porphyrins **3**, **4**, **3a** and **4a** at a final concentration of 10 μM, showed increased activity of caspase-3 enzyme compared to the negative control; indicating the induction of apoptosis. Differential gene expression pattern in SiHa cells was determined; treatments with metalloporphyrins **4a** and **4b** were performed, respectively, comparing the expression with untreated control. Treatments in both cases showed similar gene expression pattern in upregulated genes, since they share about 25 biological pathways and a large number of genes. According to the new photophysical properties related to the structural improvement and phototoxic activity, these molecules may have the potential application as photosensitizers in the photodynamic therapy.

1. Introduction

Photodynamic therapy (PDT) is a minimally invasive procedure and a promising new approach to fight cancer. PDT destroys cancer cells by photochemical generation of reactive oxygen species (ROS) mainly singlet oxygen ($^1O_2$), these species are generated by the interaction of molecular oxygen with a photosensitizing agent (PS) excited by irradiation of visible light [1]. The advantages of PDT are as follows: the PS's agents show selectivity to cancer cells; phototoxic effect is localized and occurs only in the place that is irradiated, thereby minimizing side effects; therapy can be applied repeatedly, induces an inflammatory response leading to the development of an important immune system reaction and can also be combined with other cancer treatments [2].

Porphyrins are PS's agents used in PDT. Porphyrins (aromatic macrocycles formed by four pyrrole rings joined together by interpyrrolic methine bridges) [3,4] are interesting molecules with key roles in many biological processes [5], and they have also been used for various applications, such as catalysis [6], chemical sensors [7] and photodynamic therapy [8].

An ideal photosensitizer should satisfy important requirements, such as high purity and stability, obtained by means of a simple synthesis under laboratory conditions, photoactivity at wavelengths between 630 and 800 nm, solubility in biological fluids with selective uptake in tumour cells, optimal absorption, distribution, metabolism and excretion (ADME) properties,

* Corresponding author.
E-mail address: isaias.balderasrn@uanl.edu.mx (I. Balderas-Rentería).

http://dx.doi.org/10.1016/j.biopha.2016.05.010
0753-3322/

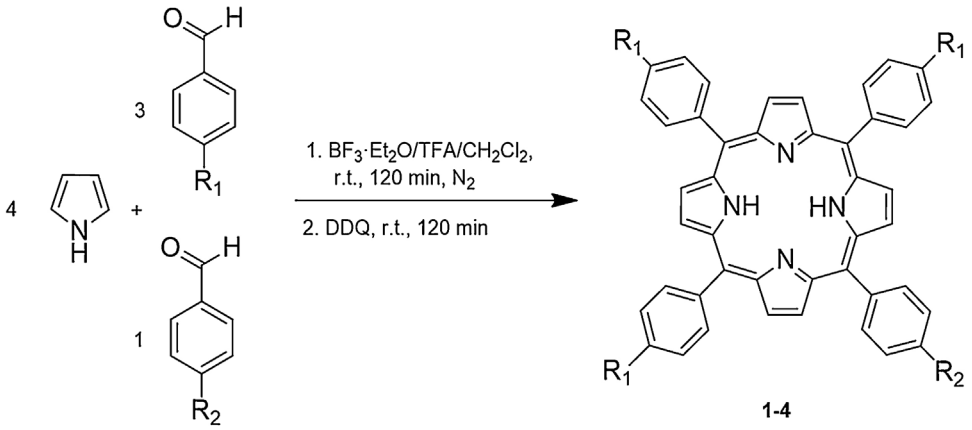

Scheme 1. Synthesis of A_3B porphyrins **1–4** by Lindsey method.

minimal toxicity in the absence of light, without yield of toxic metabolites and also no mutagenic or carcinogenic effects [9].

Porphyrins are PS's agents used in PDT, and it has been proved that the nature and location of substituents in the *meso* and β positions of the porphyrins have an effect on their spectral, photophysical and biological characteristics. Some porphyrins possess affinity for tumour cells and they absorb light in the visible range, however, high hydrophobicity is a therapeutic limitation. This problem can be solved by adding hydrophilic substituents, such as sugars, hydroxyl group, sulphates, phosphonates, peptides, etc. [10–14]. Another option for improving the properties of the photosensitizers is the formation of complexes with metals bonded inside the tetrapyrrole ring, which causes the modification of the photophysical properties of the photosensitizers [15].

In this study, we synthesized four unsymmetrical A_3B tetraaryl porphyrins; two of them functionalized with dimethyl 2-amino-pentanedioate (l-glutamate) and two obtained without any modification of the former aldehydes (*p*-methoxybenzaldehyde and methyl *p*-formylbenzoate). The corresponding zinc and copper metalloporphyrins were also obtained. We evaluated the photodynamic activity of 12 tetraaryl derivatives, four porphyrins (**1, 2, 3, 4**) and eight metalloporphyrins (**1a–4a** and **1b–4b**). The quantum yield of singlet oxygen (Φ_Δ), dark cytotoxicity, phototoxicity of all derivatives and induction of apoptosis of derivatives **3**, **3a**, **4** and **4a** was evaluated. A study of differential gene expression with DNA microarrays was also performed, and differential gene expression was compared after treatment with derivatives **4a** and **4b**.

2. Materials and methods

2.1. Materials

UV–vis measurements were performed with a Perkin Elmer Lambda-12 Spectrometer. NMR spectra were recorded on a 500 MHz Varian-NMR System, ^{1}H NMR spectra at 500 MHz with $CDCl_3$ as solvent and tetramethylsilane as internal standard. Coupling constants (*J*) are given in Hz. Mass spectrometric measurements were performed on a JEOL JMS700 instrument. CH_2Cl_2 was dried by distillation over lithium aluminium hydride. Solvents were used after distillation at normal pressure. All reactants were of reagent grade from Sigma-Aldrich and Merck as it corresponds. Chromatography glass column packed with silica gel 60 (0.04–0.063 mm) was used. We use the cell line of cervical cancer (SiHa cell) obtained from the American Type Culture Collection (ATCC) (Rockville, MD, USA), with a catalog number ATCC: HTB-35, for dark cytotoxicity, phototoxic activity, apoptosis and DNA microchip assays.

2.2. General procedure for the synthesis of unsymmetrical A_3B porphyrins

According to Geier and Lindsey [16] method, porphyrin synthesis was performed via condensation of the corresponding aromatic aldehydes and pyrrole under mixed-acid catalysis. $BF_3{\cdot}(OEt)_2$ (0.17 mg, 0.01.2 mM) and trifluoro acetic acid (TFA) (51 mg, 0.45 mM) were added to a solution of aldehyde **A** (3.75 mM), aldehyde **B** (1.25 mM) and freshly distilled pyrrole (335 mg, 5 mM) in 300 ml of CH_2Cl_2; the mixture was kept at room temperature for 2 h under inert atmosphere (N_2). Then 2,3-dichloro-5,6-dicyano-1,4-benzoquinone (DDQ) (57 mg, 0.251 mM) was added, and the mixture was kept at room temperature for 2 h. The solvent was evaporated and the crude material was purified on a chromatography column using silica gel as stationary phase and mixtures of hexanes, dichloromethane and isopropanol as eluent to give porphyrins **1–4** as purple solids (Scheme 1, Table 1).

2.2.1. 5,10,15-Tris(p-methoxyphenyl)-20-(p-methoxycarbonylphenyl)-21H,23H-porphyrin, (*1*)

The general procedure was followed using *p*-methoxybenzaldehyde as aldehyde **A** (510 mg, 3.75 mM) and methyl *p*-formylbenzoate as aldehyde **B** (205 mg, 1.25 mM), yielding 228 mg (24% yield) of **1** after column chromatography purification (hexane: dichloromethane 3:7 as eluent). UV–vis (CH_2Cl_2) λ_{max}: 423, 517, 544, 593 and 649 nm. ^{1}H NMR ($CDCl_3$) δ −2.77 (s, 2H), 4.08 (s, 9H), 4.11 (s, 3H), 7.28 (d, *J* = 7.5 Hz, 6H), 8.12 (d, *J* = 7.5 Hz, 6H), 8.3 (d, *J* = 7.5 Hz, 2H), 8.43 (d, *J* = 7.5 Hz, 2H), 8.78 (d, *J* = 4 Hz, 2H), 8.88 (s, 4H), 8.89 (d, *J* = 4 Hz, 2 H).

Table 1
Phenyl substituents in A_3B porphyrins **1–4**,synthesized by Lindsey method.

Porphyrin	R_1	R_2
1	CH_3O-	$CH_3OC(O)$-
2	$CH_3OC(O)$-	CH_3O-
3	$CH_3OC(O)$-	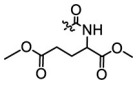
4	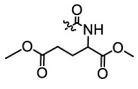	$CH_3OC(O)$-

*2.2.2. 5,10,15-Tris(*p*-methoxycarbonylphenyl)-20-(*p*-methoxyphenyl)-21H,23H-porphyrin, (**2**)*

The general procedure was followed using methyl *p*-formyl benzoate as aldehyde **A** (616 mg, 3.75 mM) and *p*-methoxybenzaldehyde as aldehyde **B** (170 mg, 1.25 mM), producing 202 mg (20% yield) of **2** after column chromatography purification (hexane:dichloromethane 3:7 as eluent). UV–vis (CH_2Cl_2) λ_{max}: 425, 516, 552, 591 and 647 nm. ^{1}H NMR ($CDCl_3$) δ −2.8 (s, 2H), 4.07 (s, 3H), 4.10 (s, 9H), 7.28 (d, J = 8 Hz, 2H), 8.11 (d, J = 8 Hz, 2H), 8.29 (d, J = 8 Hz, 6H), 8.43 (d, J = 8 Hz, 6H), 8.79 (d, J = 4.5 Hz, 2H), 8.81 (s, 4H), 8.91 (d, J = 4.5 Hz, 2H).

*2.2.3. 5,10,15-Tris(*p*-methoxyphenyl)-20-(*p*-(dimethyl-2-aminopentanedioate)-carbonylphenyl)-21H,23H-porphyrin, (**3**)*

The general procedure was followed using *p*-methoxybenzaldehyde as aldehyde **A** (510 mg, 3.75 mM) and dimethyl 2-(4-formylbenzamido)pentanedioate, **7**, as aldehyde **B** (385 mg, 1.25 mM), producing 294 mg (26% yield) of **3** after column chromatography purification (dichloromethane:isopropanol 98:2 as eluent). UV–vis (CH_2Cl_2) λ_{max}: 421, 518, 555, 593 and 649 nm. ^{1}H NMR ($CDCl_3$) δ −2.76 (s, 2H), 1.21 (q, 2H), 1.25 (t, 2H), 4.11 (s, 9H), 4.12 (s, 6H), 7.27 (d, J = 8.5 Hz, 6H), 8.14 (d, J = 8.5 Hz, 6H), 8.35 (d, J = 8.5 Hz, 2H), 8.45 (d, J = 8.5 Hz, 2H), 8.81 (d, J = 4 Hz, 2H), 8.90 (s, 4H), 8.92 (d, J = 4, 2H).

*2.2.4. 5,10,15-Tris(*p*-(dimethyl-2-aminopentanedioate)-carbonylphenyl)-20-(*p*-methoxyphenyl)-21H,23H-porphyrin, (**4**)*

The general procedure was followed using dimethyl 2-(4-formylbenzamido)pentanedioate, **7**, as aldehyde **A** (1.15 g, 3.75 mM) and *p*-methoxybenzaldehyde as aldehyde **B** (170 mg, 1.25 mM), producing 390 mg (25% yield) of **4** after column chromatography purification (dichloromethane:isopropanol 98:2 as eluent). UV–vis (CH_2Cl_2) λ_{max}: 424, 517, 557, 592 and 648 nm. ^{1}H NMR ($CDCl_3$) δ −2.77 (s, 2H), 1.25 (q, 6H), 1.28 (t, 6H), 4.10 (s, 3H), 4.12 (s, 18H), 7.27 (d, J = 8 Hz, 2H), 8.15 (d, J = 8 Hz, 2H), 8.32 (d, J = 8 Hz, 6H), 8.42 (d, J = 8 Hz, 6H), 8.81 (d, J = 4.5 Hz, 2H), 8.82 (s, 4H), 8.91 (d, J = 4.5 Hz, 2H).

2.3. General procedure for the synthesis of dimethyl 2-(4-formylbenzamido) pentanedioate

The synthetic route that includes at first the coupling reaction between *p*-formylbenzoic acid, **5**, and dimethyl 2-aminopentanodioate, **6**, following the typical conditions for amide formation (Scheme 2) [17], obtaining dimethyl 2-(*p*-formylbenzamide) pentanedioate, **7**.

2.3.1. Synthesis of p*-formyl benzoic acid, (**5**)*

Methyl *p*-formyl benzoate (1 g, 6 mM) was dissolved in 40 ml of CH_3OH and KOH (617 mg, 11 mM) was dissolved in 10 ml of H_2O, the solutions were mixed together and allowed to stir at room temperature for 18 h. The pH of the solution was adjusted to 2 by the addition of HCl (20% in CH_3OH) and then filtered. The solvent was evaporated and the crude material was purified on a chromatography column using silica gel as stationary phase and AcOEt as eluent to give 846 mg (92% yield) of *p*-formyl benzoic acid, **5**, as a beige solid. ^{1}H NMR ($CDCl_3$) δ 7.29 (d, J = 8 Hz, 2H), 8.26 (d, J = 8 Hz, 2H), 10.13 (s, 1H).

*2.3.2. Synthesis of dimethyl 2-aminopentanedioate, (**6**)*

l-glutamic acid (1 g, 7 mM) was dissolved in 30 ml of CH_3OH, and SOCl (1.19 g, 10 mM) was added dropwise. The reaction mixture was then allowed to stir at room temperature for 18 h, the solvent was evaporated and the crude product washed with ethyl ether. The product was dissolved in AcOEt, then Et_3N (506 mg, 5 mM) was added and the mixture was stirred for 18 h at room temperature, after white precipitate was formed, the reaction mixture was filtered and the solvent evaporated to give 437 mg of compound **6** (70% yield). ^{1}H NMR ($CDCl_3$) δ 2.32 (m, 2H), 2.43 (t, 2H), 3.7 (s, 6H), 4.21 (s, 2H) and 4.23 (t, 1H).

*2.3.3. Synthesis of dimethyl 2-(4-formylbenzamide)pentanedioate, (**7**)*

The synthesis was performed following the typical conditions for amide formation [21]. *p*-Formyl benzoic acid **5** (1 g, 6.6 mM) and dimethyl 2-aminopentanedioate **6** (1.76 mg, 10 mM) were placed in a flask under inert nitrogen atmosphere, then *N,N′*-dicyclohexylcarbodiimide (1.36 g, 6.6 mM) and 4-dimethylaminopyridine (147 mg, 1.2 mM) were dissolved in 40 ml of dry CH_2Cl_2, transferred via cannula into the reaction flask and then allowed to stir for 20 h at room temperature. The crude reaction was filtered and washed with AcOEt and the filtrate was evaporated. After purification on a chromatography column using silica gel as stationary phase and AcOEt as eluent, 673 mg of **7** were obtained (33% yield) as a beige solid.^{1}H NMR ($CDCl_3$) δ 2.18 (t, 2H), 2.39 (m, 2H), 3.69 (s, 3H), 3.76 (s, 3H), 4.64 (t, 1H), 6.24 (s, 2H), 7.99 (d, J = 8 Hz, 2H), 8.26 (d, J = 8 Hz, 2H), 10.11 (s, 1H)

2.4. General procedure for the synthesis of metalloporphyrins

Metalloporphyrins **1a**–**4a** and **1b**–**4b** were obtained by metallation of porphyrins with Zn(II) and Cu(II) as follows: 0.1 mM of the corresponding porphyrin were dissolved in 10 ml of CH_2Cl_2. A solution of 0.2 mM of the metal acetate in 10 ml of CH_3OH was prepared. The solutions were mixed and then stirred for 2 h at room temperature. Finally, the solvent was evaporated and the metalloporphyrins purified on a chromatography column using silica gel as stationary phase and CH_2Cl_2 as eluent (Scheme 3) [18].

*2.4.1. 5,10,15-Tris(*p*-methoxyphenyl)-20-(*p*-methoxycarbonylphenyl)-porphyrinate zinc(II) complex, (**1a**)*

The general procedure was followed using porphyrin **1** (76.23 mg, 0.1 mM) and zinc acetate (36.69 mg, 0.2 mM), producing 58 mg (71% yield) of **1a**. UV–vis (CH_2Cl_2) λ_{max}: 422, 550 and 592 nm ^{1}H NMR ($CDCl_3$) δ 4.09 (s, 9H), 4.11 (s, 3H), 7.28 (d, J = 8.7 Hz, 6H), 8.12 (d, J = 8.7 Hz, 6H), 8.29 (d, J = 8.1, 2H), 8.42 (d, J = 8.1 Hz, 2H), 8.87 (d, J = 4.8 Hz, 2H), 8.98 (s, 4H), 8.99 (d, J = 4.8 Hz, 2H).

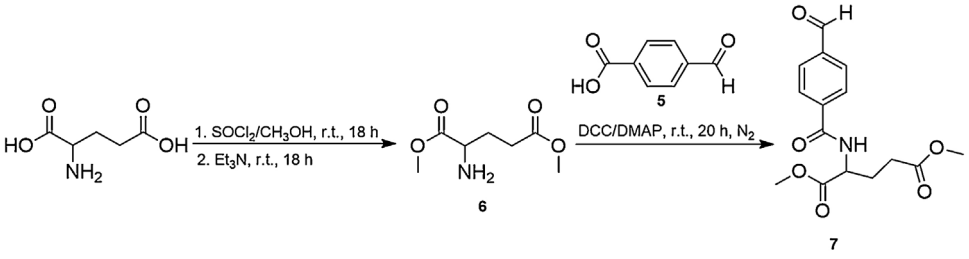

Scheme 2. Synthesis of dimethyl 2-(4 formylbenzamide) pentanedioate, **7**.

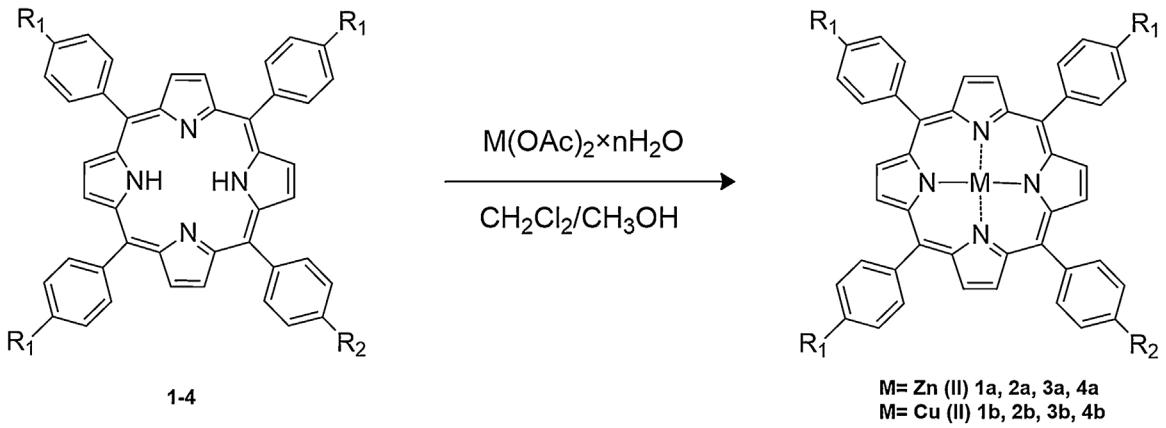

Scheme 3. Synthesis of metalloporphyrins **1a**–**4a** and **1b**–**4 b**.

*2.4.2. 5,10,15-Tris(*p-*methoxyphenyl)-20-(*p-*methoxycarbonylphenyl)-porphyrinate copper(II) complex, (**1b**)*

The general procedure was followed using porphyrin **1** (76.23 mg, 0.1 mM) and copper(II) acetate (36 mg, 0.2 mM), producing 45 mg (55% yield) of **1b**. UV–vis (CH_2Cl_2) λ_{max}: 418, 540 and 578 nm.

*2.4.3. 5,10,15-Tris(*p-*methoxycarbonylphenyl)-20-(*p-*methoxyphenyl)-porphyrinate zinc(II) complex, (**2a**)*

The general procedure was followed using porphyrin **2** (81.83 mg, 0.1 mM) and zinc acetate (37 mg, 0.2 mM), producing 72 mg (82% yield) of **2a**. UV–vis (CH_2Cl_2) λ_{max}: 420, 551 and 592 nm. ^{1}H NMR ($CDCl_3$) δ 4.09 (s, 2H), 4.10 (s, 9H), 7.28 (d, J = 8.4 Hz, 2H), 8.11 (d, J = 8.4 Hz, 2H), 8.29 (d, J = 8.1 Hz, 6H), 8.43 (d, J = 8.1 Hz, 6H), 8.88 (d, J = 4.8 Hz, 2H), 8.90 (s, 4H), 9.02 (d, J = 4.8 Hz, 2H).

*2.4.4. 5,10,15-Tris(*p-*methoxycarbonylphenyl)-20-(*p-*methoxyphenyl)-porphyrinate copper(II) complex, (**2b**)*

The general procedure was followed using porphyrin **2** (81.83 mg, 0.1 mM) and copper(II) acetate (36.32 mg, 0.2 mM), producing 75 mg (85% yield) of **2b**. UV–vis (CH_2Cl_2) λ_{max}: 417, 539 and 577 nm.

*2.4.5. 5,10,15-Tris(*p-*methoxyphenyl)-20-(*p-*(dimethyl-2-aminopentanedioate)-carbonylphenyl)-porphyrinate zinc(II) complex, (**3a**)*

The general procedure was followed using porphyrin **3** (91 mg, 0.1 mM) and zinc acetate (37 mg, 0.2 mM), producing 64 mg (67% yield) of **3a**. UV–vis (CH_2Cl_2) λ_{max}: 424, 555 and 598 nm. ^{1}H NMR ($CDCl_3$) δ 1.21 (q, 2H), 1.25 (t, 2H), 4.12 (s, 9H), 4.13 (s, 6H), 7.27 (d, J = 8.5 Hz, 6H), 8.14 (d, J = 8.5 Hz, 6H), 8.35 (d, J = 8.5 Hz, 2H), 8.45 (d, J = 8.5 Hz, 2H), 8.91 (d, J = 4 Hz, 2H), 9.01 (s, 4H), 9.02 (d, J = 4 Hz, 2H).

*2.4.6. 5,10,15-Tris(*p-*methoxyphenyl)-20-(*p-*(dimethyl-2-aminopentanedioate)-carbonylphenyl)-porphyrinate copper(II) complex, (**3b**)*

The general procedure was followed using porphyrin **3** (91 mg, 0.1 mM) and copper(II) acetate (36 mg, 0.2 mM), producing 63 mg (66% yield) of **3b**. UV–vis (CH_2Cl_2) λ_{max}: 415, 546 and 572 nm.

*2.4.7. 5,10,15-Tris(*p-*(dimethyl-2-aminopentanedioate)-carbonylphenyl)-20-(*p-*methoxyphenyl)-porphyrinate zinc(II) complex, (**4a**)*

The general procedure was followed using porphyrin **4** (125 mg, 0.1 mM) and zinc acetate (37 mg, 0.2 mM), producing 57 mg (44% yield) of **4a**. UV–vis (CH_2Cl_2) λ_{max}: 422, 550 and 591 nm. ^{1}H NMR ($CDCl_3$) δ 1.25 (q, 6H), 1.28 (t, 6H), 4.10 (s, 3H), 4.12 (s, 18H), 7.27 (d, J = 8 Hz, 2H), 8.15 (d, J = 8 Hz, 2H), 8.32 (d, J = 8 Hz, 6H), 8.42 (d, J = 8 Hz, 6H), 8.91 (d, J = 4.5 Hz, 2H), 8.92 (s, 4H), 8.98 (d, J = 4.5 Hz, 2H).

*2.4.8. 5,10,15-Tris(*p-*(dimethyl-2-aminopentanedioate)-carbonylphenyl)-20-(*p-*methoxyphenyl)-porphyrinate copper(II) complex, (**4b**)*

The general procedure using porphyrin **4** (125 mg, 0.1 mM) and copper(II) acetate (36 mg, 0.2 mM), producing 72 mg (56% yield) of **4b**. UV–vis (CH_2Cl_2) λ_{max}: 419, 540 and 575 nm was followed.

2.5. Photodynamic activity

2.5.1. Quantum yields of singlet oxygen

Quantum yields of singlet oxygen with the method of illumination in the steady state were determined, comparing the scavenger consumption rates of a reference photosensitizer and the compounds under study [19].

5,10,15,20-tetra(4-hydroxyphenyl)-porphyrin (*p*-TPPH) was used as reference photosensitizer with a quantum yield of 0.56 using methanol as solvent, 1,3-diphenylisobenzofuran (DPBF) was used as scavenger [20]. The singlet oxygen quantum yields (Φ_Δ) were calculated by the equation: Φ_Δ (sample) = (k_{sample}/k_{ref}) · (A_{ref}/A_{sample}) · $\Phi_{\Delta(ref)}$, where $\Phi_{\Delta(ref)}$ is the singlet oxygen quantum yield for the reference (*p*-TPPH) in methanol ($\Phi_{\Delta(ref)}$ = 0.56), k_{sample} and k_{ref} are the DPBF photobleaching rates in the presence of the samples and reference, respectively; A_{ref} and A_{sample} are the absorbance at Q band of the samples and reference, respectively.

Determination of Φ_Δ was performed as follows: 2.5 ml of acidified methanol was placed with an appropriate amount of the test compound to an optical density of 1.00 ± 0.02 in the Soret band. Aliquots of 1,3-diphenylisobenzofuran in acetonitrile (25 μl) were added to an optical density of 1.00 ± 0.02 at 410 nm. The solution was irradiated with visible light (LED Lamp ATLED Apollo BR40 35W true white). Finally, the optical density at 410 nm was determined at different times (25, 50, 75 and 100 s) in a GENESYS 20 spectrophotometer model (THERMO SPECTRONIC).

2.5.2. Cytotoxic studies

The phototoxic effects of the porphyrin derivatives were determined on human adenocarcinoma SiHa cells maintained in MEM supplemented with 10% fetal bovine serum at 37 °C in a humidified 5% CO_2 atmosphere. The viability study was assessed using the WST-1 assay. Briefly, 5×10^3 cells were seeded on to 96-well plates and incubated for 24 h to grow. After this incubation period, the cells were treated with different concentrations of the

compound and incubated for 24 h. Later, the medium was replaced by PBS and the cells were irradiated under visible light (LED Lamp ATLED Apollo BR40 35W true white, 0.3 m away from the culture plate) for 2 h. At the end of this time, the cells were incubated for 24 h; WST-1 (4-[3-(4-iodophenyl)-2-(4-nitrophenyl)-2H-5-tetrazolio]-1,3-benzene disulfonate) was then added to each well (10 μl) for 2 h at 37 °C. Optical densities were measured at 450 nm using a Universal Microplate Reader ELx800 (Biotek Instrument, Vermont, USA). [11]. As a positive control Triton X-100 at 1% in PBS was used, the negative control was culture medium without any treatment and as blank, reaction MEM medium and WST-1 was used, we also used a control of the solvent (isopropanol/dichloromethane, 2:1), the final concentration of solvent in each reaction well was 0.5% (v/v) or less. The dark cytotoxicity was determined as phototoxicity except that irradiation was omitted. Different concentrations of the compounds to be evaluated were prepared from a stock of 200 μM in 30 μl isopropanol/dichloromethane 2:1, and then was complete to 1 ml with medium MEM. The tested concentrations were 10, 5, 1, 0.1 and 0.01 μM.

2.5.3. Apoptosis

Activity of caspase-3 was performed as apoptosis assay following the procedure of commercial kit (The ApoTarget ™ Protease Assay Caspase-3, Invitrogen). The compound under study (**3**, **4**, **3a** and **4a**) and podophyllotoxin as positive control at a final concentration of its IC_{50} were exposed on the SiHa cells (podophyllotoxin IC_{50} 0.02 μM on Hela cells), untreated cells were used as negative control [21].

2.5.4. DNA microarrays

SiHa cells were treated for 24 h with the metalloporphyrin **4a** and **4b**, respectively, at a concentration of 10 μM. Untreated cells were used for the comparison of gene expression after treatment. The cells were incubated for 4 h, followed by the conventional RNA extraction, then the complementary DNA (cDNA) labeled with fluorophores was synthesized. The cDNA was hybridized in the microarray, after hybridization the microarray was scanned.

The RNA was extracted with Trizol reagent (Invitrogen). RNA samples were run on an agarose gel 1% to identify RNA integrity. RNA concentrations were determined with a NanoDrop (Thermoscientific) spectrophotometer. The Chipshot kit (Promega) was used, following the Promega Protocol (Z3604) −20 μg of total RNA was used to obtain aminoallyl-cDNA and subsequent purification.

To obtain quantitative values of each signal of fluorescence in the microarray slide, the image analysis was performed using the software GenArise. The upregulated and downregulated genes with a *z*-score greater or lesser than ±2 standard deviations as applicable were considered significant for the bioinformatics analysis. By means of DAVID (The Database for Annotation, Visualization program and Integrated Discovery) virtual platform, biological pathways were identified, in which upregulated and downregulated genes were presented [22].

3. Results and discussion

3.1. Synthesis and characterization

In order to obtain unsymmetrical A_3B porphyrins, **1** and **2**, we followed the procedure described by Lindsey and co-workers (Scheme 1 and Table 1), via acid-catalyzed condensation of pyrrole and the corresponding aldehydes followed by oxidation with DDQ.

The purification of each reaction mixture by chromatography column allowed us to obtain two new unsymmetrical porphyrins, **1** and **2** (24% and 20% yield, respectively).

Our interest on obtaining A_3B unsymmetrical porphyrins functionalized by amino acids lead us to propose the synthetic route that includes at first the coupling reaction between *p*-formylbenzoic acid, **5**, and dimethyl 2-aminopentanodioate, **6**, following the typical conditions for amide formation (Scheme 2), obtaining dimethyl 2-(*p*-formylbenzamide)pentanedioate, **7**, (33% yield). Dimethyl 2-aminopentanodioate **6** was previously synthesized by the esterification of l-glutamic acid, using thionyl chloride to obtain the corresponding dichloride followed by the esterification with methyl alcohol; the spectral data obtained for this product are in agreement with those described earlier [23].

Once dimethyl 2-(*p*-formylbenzamide)pentanedioate, **7**, was obtained, we finished the synthetic route obtaining functionalized unsymmetrical A_3B porphyrins, **3** and **4** (26% and 25% yield, respectively) by Lindsey procedure having *p*-methoxy benzaldehyde as the other aldehyde in the reaction mixture with pyrrole, with the corresponding stoichiometric ratio depending on which group was considered as A or B *meso* group (Scheme 1 and Table 1). This procedure is different from other reports in which the functionalized porphyrins are synthesized by first obtaining the free base porphyrin and then performing diverse types of functionalization, sometimes having disadvantages related to the reactivity of the other *meso* substituents or with the porphyrin macrocycle itself [24–26]. The route reported here could have the advantage of identifying the functionalization group since the beginning and then continue to the formation of the porphyrin macrocycle which is easily identified by the characteristic UV–vis absorption pattern, a high intensity Soret band around 420 nm and four low intensity Q bands Qy(1,0), Qy (0,0), Qx(1,0) and Qx(0,0) between 480 and 700 nm (Table 2) [3].

The H^1 NMR data of new porphyrins show all the expected signals. The free base porphyrins showed that highly shielded peak at around −2 and −3 ppm is the N—H at the center of porphyrin ligand in comparison with metalloporphyrins as this peak disappeared after complexation of porphyrin with metal because the two H atom are replaced by metal ion. The H^1 NMR data of cupper metalloporphyrins were not obtained due to paramagnetic metal nature [18]. However, the structure of all the synthesized metalloporphyrins was also assured because the former free base porphyrin in each case was characterized and there was a significant difference of the UV–vis pattern as described later. The absorption spectra of metalloporphyrins is characterized by a strong near-UV Soret band, around 420 nm, and two weaker bands, the Q(1-0) and Q(0-0), around 539 and 598 nm, these are in consequence of the square symmetry introduced by the metal (Table 2) [3,5].

It is important to notice the moderate reduction of hydrophobicity of porphyrins **3** and **4** compared with **1** and **2,** as it was observed at first by the Rfs on TLC (CH_2Cl_2-iPrOH, 98-2), **1**, Rf = 0.75,

Table 2
Photophysical properties of porphyrins and metalloporphyrins.

Porphyrin	UV–visible parameter (λ_{max}/nm)[a]		Φ_D[b] ± SD
	Soret Band	Q Bands	
1	423	517, 544, 593, 649	0.47 ± 0.05
2	425	516, 552, 591, 647	0.42 ± 0.02
3	421	518, 555, 593, 649	0.50 ± 0.04
4	424	517, 557, 592, 648	0.46 ± 0.03
1a	422	550, 592	0.66 ± 0.02
2a	420	551, 592	0.67 ± 0.03
3a	424	555, 598	0.61 ± 0.03
4a	422	550, 591	0.56 ± 0.03
1b	418	540, 578	0.21 ± 0.04
2b	417	539, 577	0.21 ± 0.03
3b	415	546, 572	0.25 ± 0.04
4b	419	540, 575	0.22 ± 0.01

[a] In dichloromethane.
[b] Using (*p*-THPP, Φ_Δ = 0.56 in methanol) as the reference.

2, Rf = 0.64, **3**, Rf = 0.35 and **4**, Rf = 0.22. We also calculate the Log *P* using Chem BioDraw®, **1**, Log *P* = 9.74, **2**, Log *P* = 9.91, **3**, Log *P* = 8.28 and **4**, Log *P* = 7.35. These two parameters suggest that porphyrins **3** and **4** are less lipophilic than **1** and **2**. The decrease in the Log *P* values modifies the balance between hydrophilic and hydrophobic character of the compounds, and the presence of l-glutamate in the structure as substituent of the *meso* groups of porphyrins **3** and **4**, improves the high hydrophobicity of porphyrin core [10–14], and it seems to be important especially for the possible application as photosensitizers and the permeation across biological membranes [27,28].

Porphyrins bearing amino acid moieties have been reported to have interesting characteristics for PDT, because of their ability to stablish specific interactions with cell membranes and to improve the solubility in aqueous solutions [29,30]. The synthesis of a cationic porphyrin modified glutamic acid protected either by an N-Boc or an N-Fmoc group was reported, emphasizing the great interest of these porphyrins as inhibitors of human telomerases, DNA intercalators, components of artificial receptors and photosensitizers in photodynamic therapy [31]. Based on these and other similar publications in which it is clear that the relevance of the presence of amino acid moieties as part of the *meso* substituents of porphyrins, the synthesis and characterization of porphyrins **3** and **4** functionalized with l-glutamate represent an important contribution.

In addition to these four new porphyrins whose photophysical and biological characteristics could be compared between each other in order to establish the effect of the glutamate functionalization group, we consider to complete the study by synthesizing the corresponding Zn(II) and Cu(II) metalloporphyrins (Scheme 3). Zinc porphyrins have been proved as good photosensitizers [32], while some copper porphyrins presented average photodynamic activity [33]. Metalloporphyrins **1a**–**4a** and **1b**–**4b** were obtained following the synthetic procedure that results in the coordination of the corresponding metal with nitrogen atoms located inside the porphyrin core, due to the reaction of the free base porphyrin with the metal salt (acetate); after purification, the metalloporphyrins were obtained in 44–85% yields.

3.2. Quantum yield of singlet oxygen

Porphyrins and metalloporphyrins presented values of Φ_Δ ranging from 0.21 to 0.67 metalloporphyrins copper **1b**, **2b**, **3b** and **4b** had the lowest of Φ_Δ values, this is because the paramagnetic metal deactivate the excited states and shorten life time of the triplet state, while zinc metalloporphyrins **1a**, **2a**, **3a** and **4a** showed the highest values of Φ_Δ, increasing the intersystem crossing and lifetime of triplet state, attributed to diamagnetic metal (Table 2) [15].

Zinc metalloporphyrins have the highest values of singlet oxygen; these values are similar to other porphyrins and metalloporphyrins presented by other authors, Cheng-Liang et al. reported Φ_Δ values between 0.45 and 0.68 for symmetrical and unsymmetrical porphyrins with *meso* substituents *p*-hydroxyphenyl and *p*-aminophenyl and Nifiatis et al. reported halogen tetraaryl porphyrins in the *meso*-phenyl group Φ_Δ values between 0.63 and 0.96 [19,32]. As reported by others, in the present work, compounds with higher values of $\Phi\Delta$ are considered better photosensitizers. The increase in the quantum yield of singlet oxygen can be attributed to the increased hydrophilicity [34,35].

3.3. Cytotoxic effects

The dark cytotoxicity of porphyrins and metalloporphyrins in SiHa cells was determined by WST-1 assay. The cells were exposed to all tetraaryl derivatives at different concentrations below 10 μM for 48 h in the dark. The results are shown in dose–response curves (Fig. 1a). Functionalized porphyrins and corresponding metallated with zinc **3**, **4**, **3a** and **4a** had the higher values of dark cytotoxicity, that could be attributed to a higher cellular uptake (not determined) [19].

Phototoxicity was also determined in SiHa cells, after cells were exposed to tetraaryl derivatives for 24 h, the cells were irradiated with visible light for 2 h (Fig. 1b). IC_{50} values were determined by extrapolating the results presented in dose-response curves (Table 3). IC_{50} values were calculated for all compounds studied. Comparing the phototoxic activity of porphyrins, it can be observed that functionalization of porphyrins with glutamate increased 100 times phototoxic activity (**1** (IC_{50} 4.81 ± 0.34 μM) vs. **3** (IC_{50} 0.04 ± 0.02 μM) and **2** (IC_{50} 5.19 ± 0.42 μM) vs. **4** (IC_{50} 0.05 ± 0.01 μM)). This increased activity can be attributed to moderate reduced hydrophobicity, increased cellular uptake and increased Φ_Δ, which is given by functionalization with glutamate. It has been reported that the addition of hydrophilic substituents increases the recognition of the membrane, cellular uptake and can address the photosensitizers to tumour cells [10,15,19,36]. Metallation with zinc increased phototoxic activity compared with the corresponding porphyrins. Metallation with copper decreased phototoxic activity compared with the corresponding porphyrins. Metalloporphyrins **3a** (IC_{50} 0.04 ± 0.01 μM) and **4a** ($IC_{50} < 0.01$ μM) presented the best values of phototoxic activity. Therefore, functionalization and zinc metallation increased phototoxic activity.

Phototoxicity results presented in this paper are similar to porphyrins synthesized and evaluated by other authors. Wang et al., functionalized meso-tetra(4-aminophenyl)porphyrin with the amino acid valine, the functionalized porphyrin showed highlighted phototoxicity (from a concentration of 1 μM) after irradiation with visible light on MCF-7 cells [30]. In a study presented by Banfi et al., synthesized seven tetraaryl porphyrins with substituents *meso* hydroxyphenyl and methoxyphenyl and phototoxic activity was evaluated in HTC 116 cells of colorectal carcinoma, IC_{50} values ranging between 0.004 and 13 μM were obtained; phototoxicity values against Photofrin®, which presented an IC_{50} of 0.073 μg/ml are compared [37]. According to these results and those presented by Banerjee et al., who reported an IC_{50} value of 4.3 μM for Photofrin® on HeLa cells [38], we can conclude that functionalized porphyrins **3** and **4** and the zinc metalloporphyrins **3a** and **4a** could be more phototoxic than Photofrin®.

Other authors also reported the activity of other photosensitizers, which are considered for most of the phototoxic photosensitizers, the *p*-THPP with an IC_{50} of 0.0045 μM to HTC 116 cells [37] and temoporfin with an IC_{50} of 0.0076 μM on the same cells [39].

The fact that the zinc metalloporphyrin **4a** presented an $IC_{50} < 0.01$ μM in SiHa cells makes it a promising PS agent. Králová et al., synthesized glycol functionalized porphyrins and assessed their activity in HL60 leukaemia cells and 4T1 breast cancer cells with IC_{50} values ranging from 0.033 to 0.093 and 0.093–0.143 μM, respectively [10]. In another study presented by Laville et al., glycosylated porphyrins were synthesized and evaluated in retinoblastoma cells with IC_{50} values between 0.06 and 0.65 μM [40]. These results are comparable to those obtained in this work.

3.4. Induction of apoptosis

The activity of caspase-3 in SiHa cells after treated with porphyrins (**3**, **4**, **3a**, **4a**) to a final concentration of 10 μM and using podophyllotoxin as positive control, was determined. Fifty μg of lysate protein were used to determine activity of such enzyme. Caspase-3 enzyme hydrolyses the substrate tetrapeptide DEVD-

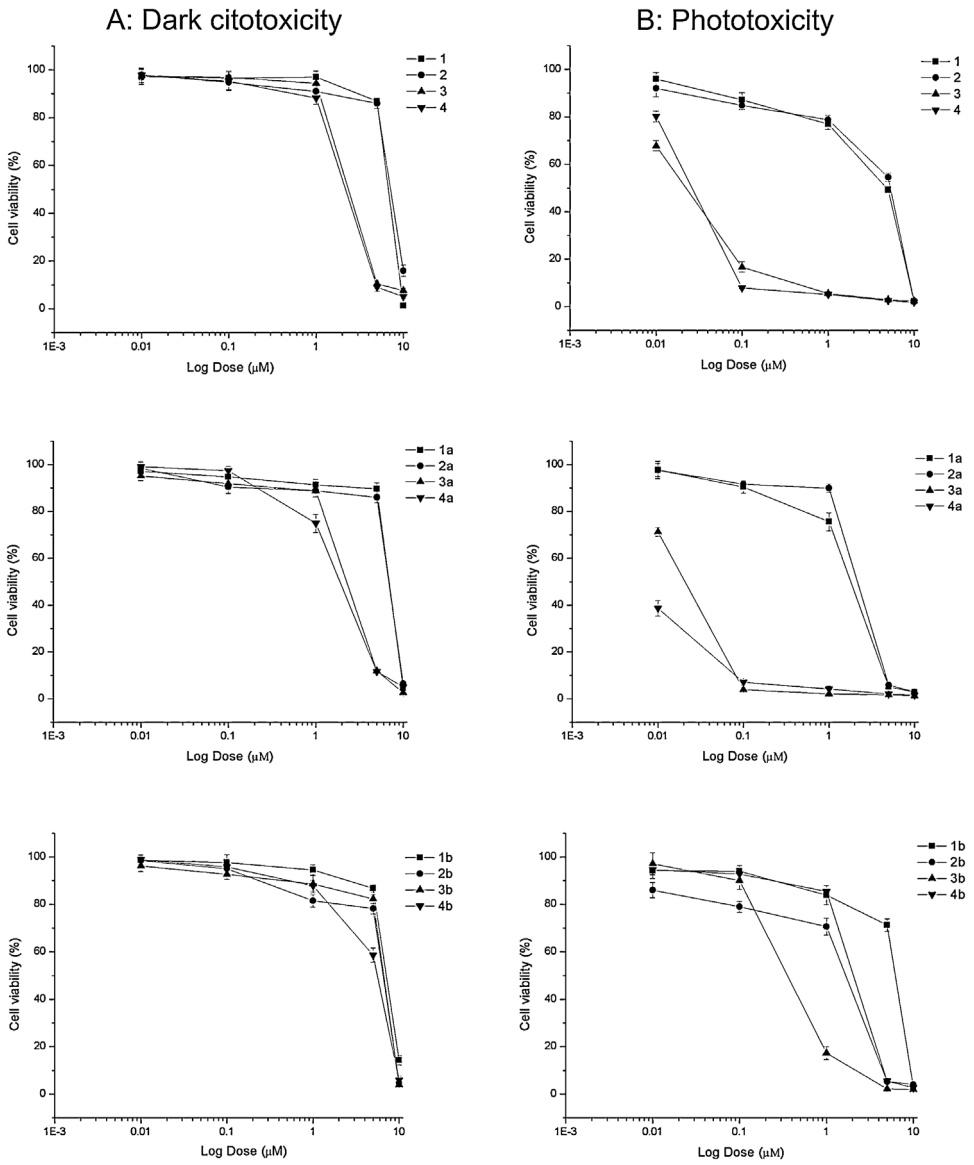

Fig. 1. Dark citotoxicity (a) and Phototoxicity (b) dose-response curve obtained in SiHa cells following exposure to different tetraayl porphyrin derivatives. Data are expressed as mean value ± standard error of the mean value of three independent experiments, each performed in quintuplicate. The colorimetric WST-1 test was used for cell viability estimation.

Table 3
IC_{50} phototoxic values of porphyrins and metalloporphyrins in SiHa cells, obtained from three different experiments with five replicates.

Porphyrin	IC_{50} (μM) ± SD	
	Dark cytotoxicity	Phototoxicity
1	7.22 ± 0.05	4.81 ± 0.34
2	7.49 ± 0.18	5.19 ± 0.42
3	3.11 ± 0.11	0.04 ± 0.02
4	2.94 ± 0.08	0.05 ± 0.01
1a	7.32 ± 0.08	2.39 ± 0.30
2a	7.25 ± 0.17	2.93 ± 0.21
3a	3.07 ± 0.27	0.04 ± 0.001
4a	2.53 ± 0.65	<0.01
1b	7.55 ± 0.13	6.56 ± 0.11
2b	6.92 ± 0.16	2.25 ± 0.04
3b	7.07 ± 0.04	0.60 ± 0.03
4b	4.82 ± 0.36	2.78 ± 0.04

*p*NA, releasing *p*-nitroaniline, which is indicative of the activity of the enzyme. The absorbance values at 405 nm are shown in Table 4. Activity of caspase-3 enzyme indicates an apoptotic process.

SiHa cells treated with porphyrins **3**, **4**, **3a** and **4a** at a final concentration of 10 μM, showed increased activity of caspase-3 enzyme compared to the negative control, but lower compared to treatment with podophyllotoxin; the activity of caspase-3 which

Table 4
Absorbance values at 405 nm indicate the activity of caspase-3 enzyme.

Treatments	Abs ± SD (405 nm)
3	0.298 ± 0.027
4	0.373 ± 0.011
3a	0.328 ± 0.033
4a	0.384 ± 0.021
Podophyllotoxin	0.489 ± 0.034
Control	0.117 ± 0.006

indicates the presence of apoptosis was observed. Apoptosis requires activation of endonucleases, DNA degradation and activation of caspases. Programmed cell death is often related to loss of mitochondrial function, which is reflected by a decrease in mitochondrial membrane potential and release of cytochrome C. It is known that the accumulation of ROS can be a cause of altered mitochondrial function. Some reports have documented the presence of apoptosis generated by the treatment of various photosensitizers [37,41,42], so the results obtained in the present work are consistent with those studies.

Inoue et al., found that treatment with 5-aminolevulinic acid decreased mitochondrial membrane potential and produce cell death caused primarily by apoptosis [43], Tochigi et al., mentioned that low concentrations of H_2O_2 activated preferably caspase-dependent apoptotic pathway while high concentrations of H_2O_2 induce both, apoptotic cell death and caspase independent necrotic process [44]. In addition, nitric oxide is involved in the photodynamic therapy, as it can either stimulate or inhibit apoptosis, acting on the NF-jB/Snail/RKIP survival/anti-apoptotic loop where low dose of PDT induces low levels of nitric oxide, which causes stimulation of the anti-apoptotic pathway after mentioned, whereas at higher doses of PDT stimulates high levels of nitric oxide, which inhibits the pathway and therefore stimulates apoptosis [45].

Kessel mentioned that overexpression of anti-apoptotic Bcl-2 protein leads to stabilization of the pro-apoptotic Bax protein. After photodamage, Bax excess is available to initiate interaction with the mitochondrial membrane, resulting in the release of cytochrome *C*; a trigger apoptosis [47], therefore the crucial factors in determining the type of cell death after PDT are: the type of cell, the subcellular localization of the PS, and the dose of light to activate the PS [47,48].

3.5. Analysis of differential gene expression (DNA microarray)

Analysing differential gene expression in SiHa cells was determined; two treatments with metalloporphyrins **4a** and **4b** were performed respectively, comparing the expression with untreated control. For treatment with metalloporphyrin **4b**, 113 genes were downregulated and 1882 genes were found as upregulated, whereas treatment with the metalloporphyrin **4a**, 45 genes were downregulated and 1841 genes were found as upregulated. A bioinformatic analysis of the upregulated and downregulated genes using the DAVID virtual tool was performed, associating these genes to metabolic and biological pathways; allowing observing changes in gene expression from treatment. For the treatment with metalloporphyrin **4a**, the tool yielded 42 biological pathways involved in the case of the upregulated genes and no interaction in biological pathways was found in down-regulated genes and treatment with metalloporphyrin **4b**, the tool yielded 35 biological pathways involved in the case of the upregulated genes and three biological pathways for down-regulated genes (Table 5).

Treatments in both cases showed similar gene expression pattern in upregulated genes since they share about 25 biological pathways and a large number of genes. This evidence may suggests that the mechanism by which the treatments have their cytotoxic activity is similar, therefore the difference in the phototoxic activity of the two treatments may be due to other factors, such as the quantum yield of singlet oxygen due to the chemical nature of the metal, the log *P*, cellular uptake, among others, and not the mechanism by which they perform their cytotoxic activity. However, results of microarrays have a qualitative character and must be verified by a quantitative technique, such as real-time PCR.

Regarding the upregulated genes, B-cell lymphoma 2 (Bcl-2 gene) was found and some studies have reported overexpression of this gene following treatment with PDT [49,50], the Bcl-2 gene controls permeability of the outer membrane after photodynamic injury, also induce the release of cytochrome *C* and, thus, induces apoptosis [46,9]. Other upregulated gene involved in apoptosis is tumour necrosis factor receptor, the signaling pathway of this receptor and FAS-associated APO2/TRIAL induces apoptosis with an independent mechanism of *p*-53 [51].

Other upregulated genes (DNA fragmentation factor 40 kDa and 45 kDa) are nucleases that mediate DNA fragmentation and chromatin condensation during apoptosis, some genes have important roles in apoptosis (caspase 6, tumour necrosis factor receptor, inhibitor of kappa light polypeptide promoter gene in B cells). Other upregulated found genes (Heat shock 70, growth arrest and Jun D) have cell function in response to stress; particularly heat shock 70 protein prevents cell death by inhibiting the aggregation of cellular proteins [50].

Upregulated genes involved in the MAPK signaling pathway was found, these enzymes are critical components of cellular

Table 5
Biological pathways shown by DAVID where the upregulated genes are involved.

Pathways	No. Upregulated genes[a]	
	Porphyrin 4a	Porphyrin 4b
Systemic lupus erythematosus	16	20
MAPK signaling pathway	25	22
Calcium signaling pathway	17	15
Prion diseases	6	5
Vascular smooth muscle contraction	12	10
Apoptosis	10	11
Long-term depression	8	7
Hedgehog signaling pathway	7	8
Ribosome	9	10
Fructose and mannose metabolism	5	–
Proteasome	6	–
Insulin signaling pathway	12	12
Adipocytokine signaling pathway	7	–
Heparan sulfate biosynthesis	4	3
Long-term potentiation	7	10
Melanogenesis	9	9
Arachidonic acid metabolism	6	–
RIG-I-like receptor signaling pathway	7	–
Phosphatidylinositol signaling system	7	–
Endocytosis	14	16
Chronic myeloid leukemia	7	8
Dilated cardiomyopathy	8	8
T cell receptor signaling pathway	9	9
Neurotrophin signaling pathway	10	–
Type II diabetes mellitus	5	–
Pathways in cancer	22	21
Ether lipid metabolism	4	–
Base excision repair	4	–
GnRH signaling pathway	8	–
Non-small cell lung cancer	5	6
Inositol phosphate metabolism	5	–
Melanoma	6	–
Gap junction	7	7
Maturity onset diabetes of the young	3	5
Dorso-ventral axis formation	3	3
VEGF signaling pathway	6	6
Starch and sucrose metabolism	4	–
Bladder cancer	4	–
Regulation of actin cytoskeleton	14	–
Axon guidance	9	12
Fc gamma R-mediated phagocytosis	7	–
Nucleotide excision repair	4	
Alzheimer's disease	–	15
Glutathione metabolism	4	6
Natural killer cell mediated cytotoxicity	–	11
Tight junction	–	10
Parkinson's disease	–	9
B cell receptor signaling pathway	–	6
Glioma	–	5

[a] Upregulated genes with a z-score greater or lesser than ± 2 SD.

signaling network that ultimately regulates gene expression in response to extracellular stimuli. The three families of MAPK are well known: the extracellular signal-regulated kinases (ERKs), protein kinases c-Jun N-terminal kinases activated by stress (JNK/SAPKs), and p38 MAPK. Each of these enzymes is a target for phosphorylation cascades wherein the sequential activation of three kinases is a common signaling pathway. The JNK and p38 proteins are key signs of stress and inflammatory mediators. Activation of the MAPK pathway appears to play an important role in the induction of apoptosis [52].

Other upregulated genes involved in the activation of apoptosis genes are the calcium signaling pathway, since it has been shown to increase intracellular calcium released from the endoplasmic reticulum and mitochondria after treatment with PDT, that it is involved in initiation and development of apoptosis [52].

Overexpression of the proto-oncogene JunD gene was also found, this gene protein complex interacts with transcription factor activator protein 1 (AP-1), whose function is related to the response to stress, differentiation and modulation of apoptosis. Other proteins encoded by the genes c-fos and c-jun, also interacting with AP-1 and were found as overexpressed genes, this in response to PDT [53].

PDT produces oxidative stress, which can result in the activation and translocation of nuclear factor kappa (NF-kB) to the core; once this take place, the biological process is directed to overexpression of genes involved in immuneregulation, proinflammatory response, anti-apoptotic genes and regulatory NF-kB negatives.The mechanism by which PDT induces translocation of NF-kB to the nucleus is unclear so far, but the NF-kB provides anti-apoptotic cells exposed to PDT signal [51]. In this study, the gene promoter inhibitor of kappa light polypeptide gene upregulated in B cells, evidence of activation of NF-kB was found. Another important pathway in response to stress is undoubtedly the metabolism of glutathione (glutathione peroxidase 4, 5, 7, etc.), these enzymes catalyze the reduction of H_2O_2 reactive oxygen species that is usually generated in photodynamic therapy [54].

4. Conclusions

Functionalization of the porphyrin with l-glutamate increases phototoxic activity observing a moderate reduction in lipophilicity of porphyrins **3** and **4** compared to **1** and **2**. Metallation of porphyrins with zinc also increases the phototoxic activity; which is related with the highest values of $\Phi\Delta$ of zinc metalloporphyrins. These changes in the structure of the studied molecules improved its phototoxic activity probably by some reduction of lipophilicity and the presence of diamagnetic metal whose effect is about increasing the intersystem crossing and the lifetime of triplet state. The porphyrins **3**, **4**, **3a** and **4a** showed induction of apoptosis compared to the negative control. The analysis of differential gene expression showed some upregulated genes that have important roles in apoptosis, inflammation, response to stress, and oxidative stress. This evidence suggests its possible application as photosensitizers in photodynamic therapy.

Acknowledgements

The authors thank CONACYT-MEXICO (project 180854) for the financial support, also thank Erick Cuevas, Victoria Labastida, Carolina Martinez and Hugo Salas for their technical support. Authors thank to Lorena Chávez, José Luis Santillán, Simón Guzmán and Jorge Ramírez for the Microarray; E.U.A.E. also thanks CONACYT for the Postgraduate scholarship (228173).

References

[1] L. Benov, Photodynamic therapy: current status and future directions, Med. Princ. Pract. 24 (2015) 14–28, doi:http://dx.doi.org/10.1159/000362416.
[2] A. O'Connor, W. Gallagher, A. Byrne, Porphyrin and nonporphyrin photosensitizers in oncology: preclinical and clinical advances in photodynamic therapy, Photochem. Photobiol. 85 (2009) 1053–1074, doi:http://dx.doi.org/10.1111/j.1751-1097.2009.00585.x.
[3] L.R. Milgrom, The Colours of Life: An Introduction to the Chemistry of Porphyrins and Related Compounds, Oxford University Press Inc., New York, 1997.
[4] M.O. Senge, Nucleophilic substitution as a tool for the synthesis of unsymmetrical porphyrins, Acc. Chem. Res. 38 (2005) 733–743, doi:http://dx.doi.org/10.1021/ar0500012.
[5] A.E.H. Machado, W.R. Gomes, D.M.S. Araújo, H.S. Miglio, L.T. Ueno, R. De Paula, J.A.S. Cavaleiro, N.M. Barbosa Neto, Synthesis and spectroscopic characterization of two tetrasubstituted cationic porphyrin derivatives, Molecules 16 (2011) 5807–5821, doi:http://dx.doi.org/10.3390/molecules16075807.
[6] A.R. McDonald, N. Franssen, G.P.M. Van Klink, G. Van Koten, 'Click' silica immobilisation of metallo-porphyrin complexes and their application in epoxidation catalysis, J. Organomet. Chem. 694 (2009) 2153–2162, doi:http://dx.doi.org/10.1016/j.jorganchem.2009.02.020.
[7] F.J. Pavinatto, A.F. Gameiro Jr., A.A. Hidalgo, L.R. Dinelli, L.L. Romualdo, A.A. Batista, N.M. Barbosa Neto, M. Ferreira, O.N. Oliveira Jr., Langmuir and Langmuir–Blodgett (LB) films of tetrapyridyl metalloporphyrins, Appl. Surf. Sci. 254 (2008) 5946–5952, doi:http://dx.doi.org/10.1016/j.apsusc.2008.03.162.
[8] V. Rapozzi, S. Zorzet, M. Zacchigna, E. Pietra, S. Cogoi, L. Xodo, Anticancer activity of cationic porphyrins in melanoma tumour-bearing mice and mechanistic *in vitro* studies, Mol. Cancer. 13 (75) (2014) 1–17, doi:http://dx.doi.org/10.1186/1476-4598-13-75.
[9] P. Agostinis, K. Berg, K.A. Cengel, T.H. Foster, A.W. Girotti, S.O. Gollnick, S.M. Hahn, M.R. Hamblin, A. Juzeniene, D. Kessel, M. Korbelik, J. Moan, P. Mroz, D. Nowis, J. Piette, B.C. Wilson, J. Golab, Photodynamic therapy of cancer: an update, CA Cancer J. Clin. 61 (2011) 250–281, doi:http://dx.doi.org/10.3322/caac.20114.
[10] J. Králová, T. Bříza, I. Moserová, B. Dolenský, P. Vašek, P. Poučkova, Z. Kejik, R. Kaplánek, P. Martásek, M. Dvořák, V. Kral, Glycol porphyrin derivatives as potent photodynamic inducers of apoptosis in tumor cells, J. Med. Chem. 51 (2008) 5964–5973, doi:http://dx.doi.org/10.1021/jm8002119.
[11] K. Nawalany, A. Rusin, M. Kepczynski, P. Filipczak, M. Kumorek, B. Kozik, H. Weitman, B. Ehrenberg, Z. Krawczyk, M. Nowakowska, Novel nanostructural photosensitizers for photodynamic therapy: in vitro studies, Int. J. Pharm. 430 (2012) 129–140, doi:http://dx.doi.org/10.1016/j.ijpharm.2012.04.016.
[12] J.T.F. Lau, P.C. Lo, W.P. Fong, D.K.P. Ng, A Zinc(II) phthalocyanine conjugated with an oxaliplatin derivative for dual chemo- and photodynamic therapy, J. Med. Chem. 55 (2012) 5446–5454, doi:http://dx.doi.org/10.1021/jm300398q.
[13] M.R. Saboktakin, R.M. Tabatabaei, A. Maharramov, M.A. Ramazanov, Synthesis and in vitro studies of biodegradable modified chitosan nanoparticles for photodynamic treatment of cancer, Int. J. Biol. Macromol. 49 (2011) 747–751, doi:http://dx.doi.org/10.1016/j.ijbiomac.2011.08.031.
[14] M. Vicente, K. Smith, Syntheses and functionalizations of porphyrin macrocycles, Curr. Org. Synth. 11 (1) (2014) 3–28, doi:http://dx.doi.org/10.2174/1385272003376346.
[15] L.B. Josefsen, R.W. Boyle, Photodynamic therapy: novel third-generation photosensitizers one step closer? Met. Based Drugs 154 (2008) 1–3, doi:http://dx.doi.org/10.1038/bjp.2008.98.
[16] G.R. Geier III, J.S. Lindsey, Effects of diverse acid catalysts on the reaction course in the two-step one-flask synthesis of meso-tetraphenylporphyrin, J. Porphyr. Phthalocyanines 6 (186) (2002) 186–197, doi:http://dx.doi.org/10.1142/S1088424602000208.
[17] S. MacMahon, R. Fong II, P.S. Baran, I. Safonov, S.R. Wilson, D.I. Schuster, Synthetic approaches to a variety of covalently linked porphyrin-fullerene hybrids, J. Org. Chem. 66 (2001) 5449–5455, doi:http://dx.doi.org/10.1021/jo010317x.
[18] B.P. Bandgar, P.B. Gujarathi, Synthesis and characterization of new meso-substituted unsymmetrical metalloporphyrins, J. Chem. Sci. 120 (2) (2008) 259–266, doi:http://dx.doi.org/10.1007/s12039-008-0031-2.
[19] P. Cheng-Liang, L. Ping-Shan, S. Ming-Jium, Influence of substitutions in asymmetric porphyrins on intracellular uptake, subcellular localization and phototoxicity in HeLa cells, Biomed. Eng. Appl. Basis Commun. 20 (2008) 9–17, doi:http://dx.doi.org/10.4015/S1016237208000556.
[20] R. Bonnett, D.J. McGarvey, A. Harriman, E.J. Land, T.G. Truscott, U. Winfield, Photophysical properties of meso-tetraphenylporphyrin and some meso-tetra (hydroxyphenyl) porphyrins, J. Photochem. Photobiol. 48 (1988) 271–276, doi:http://dx.doi.org/10.1111/j.1751-1097.1988.tb02820.x.
[21] I.V. Magedov, M. Manpadi, S.V. Slambrouck, W.F. Steelant, E. Rozhkova, N.M. Przheval'skii, S. Rogelj, A. Kornienko, Discovery and investigation of antiproliferative and apoptosis-inducing properties of new heterocyclic podophyllotoxin analogues accessible by a one-step multicomponent synthesis, J. Med. Chem. 50 (2007) 5183–5192, doi:http://dx.doi.org/10.1021/jm070528f.

[22] D. Huang, B. Sherman, R. Lempicki, Systematic and integrative analysis of large gene lists using DAVID bioinformatics resources, Nat. Protoc. 4 (2009) 1–43, doi:http://dx.doi.org/10.1038/nprot.2008.211.
[23] R. Varala, S.R. Adapa, A practical and efficient synthesis of thalidomide via Na/Liquid NH_3 methodology, Org. Process Res. Dev. 9 (2005) 853–856, doi:http://dx.doi.org/10.1021/op050129z.
[24] S.K. Pushpan, S. Venkatraman, V.G. Anand, J. Sankar, D. Parmeswaran, S. Ganesan, T.K. Chandrashekar, Porphyrins in photodynamic therapy—a search for ideal photosensitizers, Curr. Med. Chem. Anticancer Agent 2 (2002) 187–207, doi:http://dx.doi.org/10.2174/1568011023354137.
[25] S.K. Pandey, X. Zheng, J. Morgan, J.R. Missert, T.H. Liu, M. Shibata, D.A. Bellnier, A.R. Oseroff, B.W. Henderson, T.J. Dougherty, R.K. Pandey, Purpurinimide carbohydrate conjugates: effect of the position of the carbohydrate moiety in photosensitizing efficacy, Mol. Pharm. 4 (2007) 448–464, doi:http://dx.doi.org/10.1021/mp060135x.
[26] K. Stefflova, H. Li, J. Chen, G. Zheng, Peptide-based pharmacomodulation of a cancer-targeted optical imaging and photodynamic therapy agent, Bioconjugate Chem. 18 (2007) 379–388, doi:http://dx.doi.org/10.1021/bc0602578.
[27] H. Taima, A. Okubo, N. Yoshioka, H. Inoue, Synthesis of cationic water-soluble esters of chlorin e6, Tetrahedron Lett. 46 (2005) 4161–4164, doi:http://dx.doi.org/10.1016/j.tetlet.2005.04.069.
[28] G. Garcia, V. Sol, F. Lamarche, R. Granet, M. Guilloton, Y. Champavier, P. Krausz, Synthesis and photocytotoxic activity of new chlorin–polyamine conjugates, Bioorg. Med. Chem. Lett. 16 (2006) 3188–3192, doi:http://dx.doi.org/10.1016/j.bmcl.2006.03.044.
[29] V. Vaz Serra, A. Zamarrón, M.A.F. Faustino, M.C. Iglesias-de la Cruz, A. Blázquez, J.M.M. Rodrigues, M.G.P.M.S. Neves, J.A.S. Cavaleiro, A. Juarranz, F. Sanz-Rodríguez, New porphyrin amino acid conjugates: synthesis and photodynamic effect in human epithelial cells, Bioorg. Med. Chem. 18 (2010) 6170–6178, doi:http://dx.doi.org/10.1016/j.bmc.2010.06.030.
[30] H.M. Wang, J.Q. Jiang, J.H. Xiao, R.L. Gaoa, F.Y. Lin, X.Y. Liu, Porphyrin with amino acid moieties: a tumor photosensitizer, Chem. Biol. Interact. 172 (2008) 154–158, doi:http://dx.doi.org/10.1016/j.cbi.2007.11.016.
[31] E. Biron, N. Voyer, Synthesis of cationic porphyrin modified amino acids, Chem. Commun. 37 (2005) 4652–4654, doi:http://dx.doi.org/10.1039/b508380j.
[32] F. Nifiatis, J.C. Athas, K.D. Gunaratne, Y. Gurung, K.M. Monette, P.J. Shivokevich, Substituent effects of porphyrin on singlet oxygen generation quantum yields, Open Spectrosc. J. 5 (2011) 1–12, doi:http://dx.doi.org/10.2174/1874383801105010001.
[33] L. Jayashankar, B. Syama Sundar, R. Vijayaraghavan, K.S. Betanabhatla, A.J.M. Christina, J. Athimoolam, K.S. Saravanan, Evaluation of photodynamic activity of metalloporphyrins on human neuroblastoma cell line, Pharmacologyonline 1 (2008) 66–77.
[34] R. Venkatesan, N. Periasamy, T. Srivastava, Singlet molecular oxygen quantum yield measurements of some porphyrins and metalloporphyrins, Proc. Indian Acad. Sci. 104 (1992) 713–722.
[35] A. Ogunsipe, D. Maree, T. Nyokong, Solvent effects on the photochemical and fluorescence properties of zinc phthalocyanine derivatives, J. Mol. Struct. 650 (2003) 131–140, doi:http://dx.doi.org/10.1016/S0022-2860(03)00155-8.
[36] S. Weimin, Z. Gen, D. Guifu, Z. Yunxiao, Z. Jin, T. Jinchao, Synthesis and in vitro PDT activity of miscellaneous porphyrins with amino acid and uracil, Bioorg. Med. Chem. 6 (2008) 5665–5671, doi:http://dx.doi.org/10.1016/j.bmc.2008.03.063.
[37] S. Banfi, E. Caruso, S. Caprioli, L. Mazzagatti, G. Canti, R. Ravizza, M. Gariboldi, E. Monti, Photodynamic effects of porphyrin and chlorin photosensitizers in human colon adenocarcinoma cells, Bioorg. Med. Chem. 12 (2004) 4853–4860, doi:http://dx.doi.org/10.1016/j.bmc.2004.07.011.
[38] S. Barnajje, P. Prasad, A. Hussain, I. Khan, P. Kondaiah, A.R. Chakravarty, Remarkable photocytotoxicity of curcumin in HeLa cells in visible light and arresting its degradation on oxovanadium(IV) complex formation, Chem. Commun. 48 (2012) 7702–7704, doi:http://dx.doi.org/10.1039/c2cc33576j.
[39] S. Banfi, E. Caruso, L. Buccafurni, M. Murano, E. Monti, M. Gariboldi, E. Papa, P.J. Gramatica, Comparison between 5,10,15,20-tetraaryl- and 5,15-diarylporphyrins as photosensitizers: synthesis, photodynamic activity, and quantitative structure-activity relationship modeling, Med. Chem. 49 (2006) 3293–3304, doi:http://dx.doi.org/10.1021/jm050997m.
[40] I. Laville, S. Pigaglio, J. Blais, F. Doz, B. Loock, P. Maillard, D. Grierson, J. Blais, Photodynamic efficiency of diethylene glycol-linked glycoconjugated porphyrins in human retinoblastoma cells, J. Med. Chem. 49 (2006) 2558–2567, doi:http://dx.doi.org/10.1021/jm0580151.
[41] A. Szurko, G. Krämer-Marek, M. Widel, A. Ratuszna, J. Habdas, P. Kuś, Photodynamic effects of two water soluble porphyrins evaluated on human malignant melanoma cells *in vitro*, Acta Biochim. Pol. 50 (4) (2003) 1165–1174.
[42] M. Wawrzynska, W. Kałas, D. Biały, E. Zioło, J. Arkowski, W. Mazurek, L. Strządala, *In vitro* photodynamic therapy with chlorin e6 leads to apoptosis of human vascular smooth muscle cells, Arch. Immunol. Ther. Exp. 58 (2010) 65–75, doi:http://dx.doi.org/10.1007/s00005-009-0054-5.
[43] K. Inoue, H. Fukuhara, A. Kurabayashi, M. Furihata, M. Tsuda, K. Nagakawa, H. Fujita, K. Utsumi, T. Shuin, Photodynamic therapy involves an antiangiogenic mechanism and is enhanced by ferrochelatase inhibitor in urothelial carcinoma, Cancer Sci. 104 (2013) 765–772, doi:http://dx.doi.org/10.1111/cas.12147.
[44] M. Tochigi, T. Inoue, M. Suzuki-Karasaki, T. Ochiai, C. Ra, Y. Suzuki-Karasaki, Hydrogen peroxide induces cell death in human TRAIL-resistant melanoma through intracellular superoxide generation, Int. J. Oncol. 42 (2013) 863–872, doi:http://dx.doi.org/10.3892/ijo.2013.1769.
[45] V. Rapozzi, E.D. Pietra, S. Zorzet, M. Zacchigna, B. Bonavida, L.E. Xodo, Nitric oxide-mediated activity in anti-cancer photodynamic therapy, Nitric Oxide 30 (2013) 26–35, doi:http://dx.doi.org/10.1016/j.niox.2013.01.002.
[46] D. Kessel, Death pathways associated with photodynamic therapy, Med. Laser Appl. 21 (2006) 219–224, doi:http://dx.doi.org/10.1016/j.mla.2006.05.006.
[47] A.P. Castano, T.N. Demidovaa, M.R. Hamblin, Mechanisms in photodynamic therapy: part two cellular signaling, cell metabolism and modes of cell death, Photodiagn. Photodyn. 2 (2005) 1–23, doi:http://dx.doi.org/10.1016/S1572-1000(05)00030-X.
[48] Y. Miki, J. Akimoto, S. Yokoyama, T. Homma, M. Tsutsumi, J. Haraoka, K. Hirano, M. Beppua, Photodynamic therapy in combination with talaporfin sodium induces mitochondrial apoptotic cell death accompanied with necrosis in glioma cells, Biol. Pharm. Bull. 36 (2013) 215–221, doi:http://dx.doi.org/10.1248/bpb.b12-00567.
[49] A. Garg, D. Nowis, J. Golab, P. Agostinis, Photodynamic therapy: illuminating the road from cell death towards anti-tumour immunity, Apoptosis 15 (9) (2010) 1050–1071, doi:http://dx.doi.org/10.1007/s10495-010-0479-7.
[50] A. Castano, P. Mroz, M. Hamblin, Photodynamic therapy and anti-tumour immunity, Nat. Rev. Cancer 6 (2006) 535–545, doi:http://dx.doi.org/10.1038/nrc1894.
[51] P. Mroz, A. Yaroslavsky, G.B. Kharkwal, M.R. Hamblin, Cell death pathways in photodynamic therapy of cancer, Cancers 3 (2011) 2516–2539, doi:http://dx.doi.org/10.3390/cancers3022516.
[52] I. Moserova, J. Kralova, Role of ER stress response in photodynamic therapy: ROS generated in different subcellular compartments trigger diverse cell death pathways, PLoS One 7 (2012) 1–16, doi:http://dx.doi.org/10.1371/journal.pone.0032972.
[53] P. Wild, R. Krieg, J. Seidl, R. Stoehr, K. Reher, C. Hofmann, J. Louhelainen, A. Rosenthal, A. Hartmann, C. Pilarsky, A.K. Bosserhorf, R. Knuechel, RNA expression profiling of normal and tumor cells following photodynamic therapy with 5-aminolevulinic acid–induced protoporphyrin IX *in vitro*, Mol. Cancer Ther. 4 (2005) 516–528, doi:http://dx.doi.org/10.1158/1535-7163.MCT-04-0141.
[54] A. Casasa, G. Di Venosaa, T. Hasanb, A. Batllea, Mechanisms of resistance to photodynamic therapy, Curr. Med. Chem. 18 (16) (2011) 2486–2515, doi:http://dx.doi.org/10.2174/092986711795843272.